Aerodynamic Analysis of Micro Aerial Vehicle Rotor Blade at Low Reynolds Number

Md. Kamruzzaman[1], Sushil Nepal[2] and Mushfiq Al Arafa[3]
[1&2]Nanjing University of Aeronautics and Astronautics, China
[3]Ruhr University Bochum, Germany
E-mail: kamruzzamanshafi@outlook.com, nepalsushil@outlook.com, mushfiq.arafa@ruhr-uni-bochum.de

Abstract - The numerical simulation of micro aerial vehicle (MAV) rotor blade aerodynamics is highly challenging in the field of rotor aerodynamics. The aim of this paper is to present a computational fluid dynamics (CFD) study on the aerodynamics analysis of micro aerial vehicle rotor blade at low-Reynolds number by means of Spalart-Allmaras turbulence model. The KA152313 airfoil, which is dedicated to mid to small-scale rotorcraft, e.g. MAV is chosen to design the rotor blade. The rotor blade was investigated in three different pitch configurations, which are GP13º, GP12º and GP11º and the aerodynamics characteristics are analyzed respectively. The CFD results of the analysis is used to compare the aerodynamic characteristics, e.g. pressure force, shear force and pitching moment on the chord surface of the rotor blades at different pitch configurations.

Keywords: Micro Aerial Vehicle, Low Reynolds Number, Computational Fluid Dynamics, Rotor Blade

Nomenclature

MAV Micro Aerial Vehicle
GP   Grip
CAD Computer Aided Design
R   Radius
AoA   Angle of Attack

I. INTRODUCTION

Over the years, research field of MAV is getting prominent, as the demand of small-scale flight vehicles with multi-operational capability is increasing drastically [1]. The simultaneous usage of MAV, as shown in Fig. 1 are seen in both civilian and military aviation sectors, such as ground surveillance, payload or cargo carriers, traffic control, and geological surveying applications etc [2].

MAVs that hover in the air in a stationary position have to typically deal with low Reynolds numbers (10^3-10^5). Furthermore, extended research also indicates that, MAV can be also used for Mars operations, operating at even ultra-low-Reynolds number [3]. The rotor performances are continuously improved, in order to establish rotorcraft as a safe and competitive form of transportation. [4].

Fig. 1 Fixed-wing MAV (left) and rotor MAV (right)

II. DESIGN PROCESS OF THE ROTOR BLADE

The most significant component of rotor MAV is the rotor blade, which is responsible for the lift generation. Therefore, the selection of the rotor blade airfoil is quite important and it should be selected by considering various factors, such as: Airfoil Shape, the Reynolds Number (Re) and Mach Number (Mach). The airfoil can be chosen over the existing ones, which already have good investigation results or design a new airfoil with desirable characteristics [5]. There are many different parameters to design a rotor blade. The most important of them are the four special criteria, they are: airfoil, chord distribution, quarter chord and twist distribution. The blade airfoil selection is carried out and then the three dimensional model of the rotor blade is designed with a state of the art commercial CAD package, as shown in Fig. 3 and 4.

A. Blade Airfoil Selection
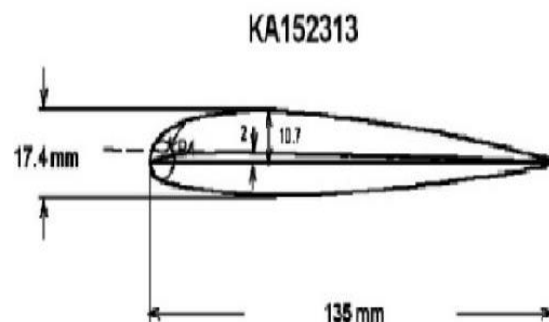
Fig. 2 KA152313 (airfoil)

The airfoil used in this simulation is KA152313, as shown in Fig. 2, which is designated to the National Advisory Committee for Aeronautics (NACA) system. The KA152313 airfoil has satisfactory performance in different AoA [6], and its specification is shown in Table I.

TABLE I SPECIFICATION OF AIRFOIL KA152313 PARAMETERS

Airfoil	Chord Length (mm)	Maximum Thickness (mm)	Chamber (mm)	Leading-edge Radius (mm)
KA152313	135	17.4	2	4

B. Rotor Blade Design

The blade of the rotor is divided into 12 sections, where each section is set at a distance of 100 mm.

The design process starts from section 12, which is known as the "grip" of the blade and ends in section 1, known as the "tip" of the rotor blade. The distance between the hub/pin (the center point around which the blade will rotate) and the grip is 400 mm or 0.4m. Then, the twist distribution is determined by applying AoA of the airfoil for each section. The KA152313 rotor blade used pitch angle at the grip (GP) of 12º, as the AoA of each section. Although, the designed rotor blade is not completely identical to the original blade, but considering that they are nearly similar, nominal GP12º is taken as the reference value for the blade design. The same design process is also carried out to obtain the other configurations with pitchconfigurationsGP13º and GP11° respectively. The twist distribution of the blade for three different pitch configurations is clearly illustrated in Table II, Table III and Table IV.

TABLE II TWIST DISTRIBUTION OF THE ROTOR BLADE AT GP13º

Section	R1(TIP)	R2	R3	R4	R5	R6	R7	R8	R9	R10	R11	R12(GP)
AoA(º)	7.5	8	8.5	9	9.5	10	10.5	11	11.5	12	12.5	13
Distance(mm) from pin	1400	1300	1200	1100	1000	900	800	700	600	500	400	300

TABLE III TWIST DISTRIBUTION OF THE ROTOR BLADE AT GP12º

Section	R1(TIP)	R2	R3	R4	R5	R6	R7	R8	R9	R10	R11	R12(GP)
AoA(º)	6.5	7	7.5	8	8.5	9	9.5	10	10.5	11	11.5	12
Distance(mm) from pin	1400	1300	1200	1100	1000	900	800	700	600	500	400	300

TABLE IV TWIST DISTRIBUTION OF THE ROTOR BLADE AT GP11º

Section	R1(TIP)	R2	R3	R4	R5	R6	R7	R8	R9	R10	R11	R12(GP)
AoA(º)	5.5	6	6.5	7	7.5	8	8.5	9	9.5	10	10.5	11
Distance(mm) from pin	1400	1300	1200	1100	1000	900	800	700	600	500	400	300

Fig. 3 Rotor Blade

Fig. 4 Rotor Blade from the Tip Side

III. MULTI-BLOCK MESH GENERATION

The grid generation process is typically extremely complex and involves dedicated software resources to help identify grids that confirm solid surfaces with a minimum degree of regularity. The quality of the mesh is of vital importance for CFD simulations in today's state of the art CAE software's.

A. Multiple Reference Frame Model (MRF)

Multiple Reference Frame (MRF) is a potential and effective steady-state CFD modelling technique, used to simulate a rotating object [7]. MRF assumes that a constant speed of rotation on a specified volume is applied, and the non-wall boundaries are revolutionary surfaces, and also assuming a weak relation between the MRF volume and the stationary volumes that surround it. Previous studies also prefer to use the sliding mesh method to measure the flow field to solve unsteady interactions [8].

The fluid domain is divided into two small-blocks. The internal block, shown in Fig. 5, Fig. 6, formed by surrounding the rotor blade and it acts as a rotational block, and the external block, shown in Fig. 7, formed by surrounding the rotational block and it is stationary. The quality of the 2D mesh along the blade surface is shown in Fig. 8 and Fig. 9.
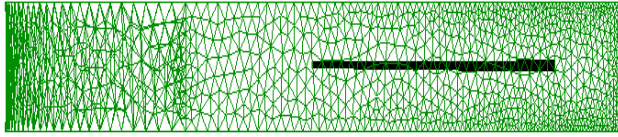
Fig. 5 Internal Block with the blade (side view)
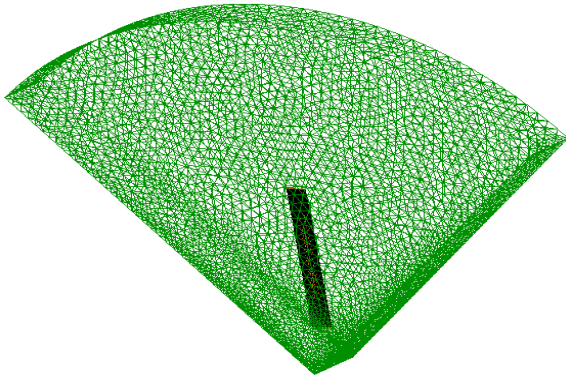
Fig. 6 Internal Block (angle view)
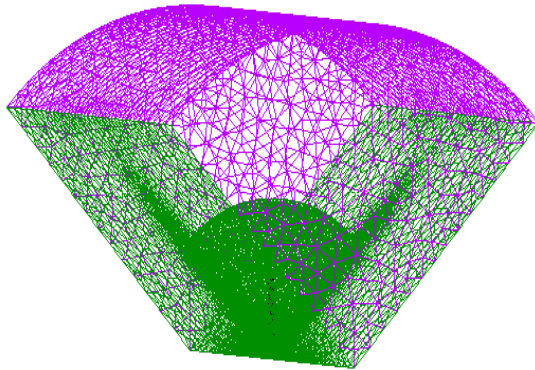
Fig. 7 External Block (angle view)
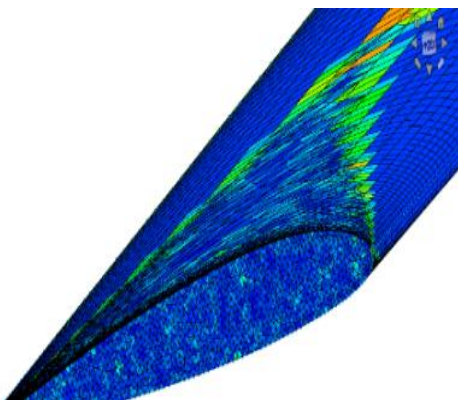
Fig. 8 Mesh Quality around the surface of the tip
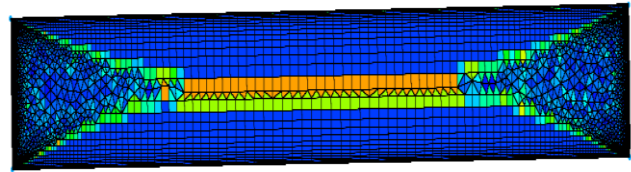
Fig. 9 Mesh Quality on the Mesh Surface

The critical area of the mesh comprises the volume mesh of the internal block, which consists the rotating fluid and the external block, which is stationary. Since important data is collected for the rotating blade, the quality mesh in these two blocks has to be adequate. Therefore, the hybrid mesh technique is applied in the rotating domain, as shown in Fig. 10 and unstructured mesh in the stationary domain. Additionally, in order to obtain better resolution of the simulation results for the vortex area, an unstructured triangle mesh was applied.
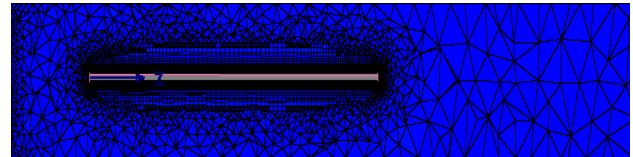
Fig. 10 Volume Mesh Quality in the Rotating Block

IV. NUMERICAL SIMULATION AND ANALYSIS

The aim of this paper is to analyze the rotor blade aerodynamics behavior in low Reynolds number at different pitch configurations. The aerodynamics characteristics are greatly influenced by the propeller's wake, which is basically turbulent in nature. Additionally, at low Reynold numbers fluid particles don't have enough energy to overcome the adverse pressure gradient in the boundary layer, as a result forming a turbulent regime in the separation bubble.

Therefore, the robust turbulence model Spalart Almaras is used to capture a detailed mode of the specified turbulent flow regions. The temperature, pressure distribution of the blade surface, x vorticity at the blade tip, lift generation at different pitch configurations is compared.

A. Comparison of Blade Temperature Distribution at Different Pitch Configurations

The temperature distribution on the upper surface and lower surface of the rotor blade is depicted in Fig. 11 and Fig. 12 respectively.

The temperature distribution at the different radius of the blade and in different pitches is shown in Fig. 13. It can be observed that the temperature difference between the lower and upper surface of the blade is very small, close to almost 1 Kelvin (K). The temperature difference between the lower and upper surface of the blade at GP12º is less compared to both the GP11º and GP13º configurations.

a) GP 13º   b) GP 12º   c) GP 11
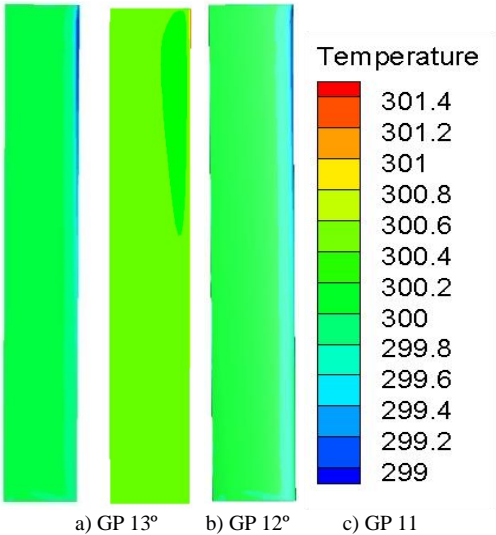
Fig. 11 Temperature Distribution on the upper surface of the Rotor Blade

a) GP 13º   b) GP 12º   c) GP 11º
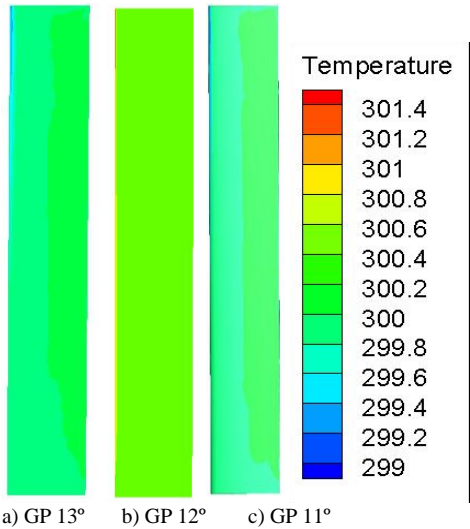
Fig. 12 Temperature Distribution on the lower surface of the Rotor Blade
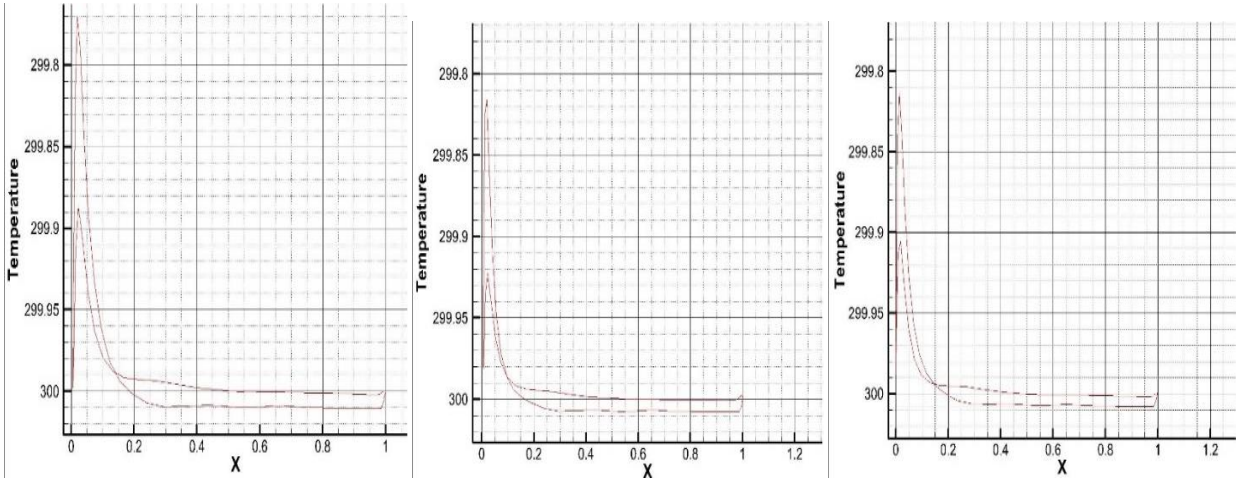
a) 0.06R (GP 13º, GP 12º, GP 11º; from left to right)
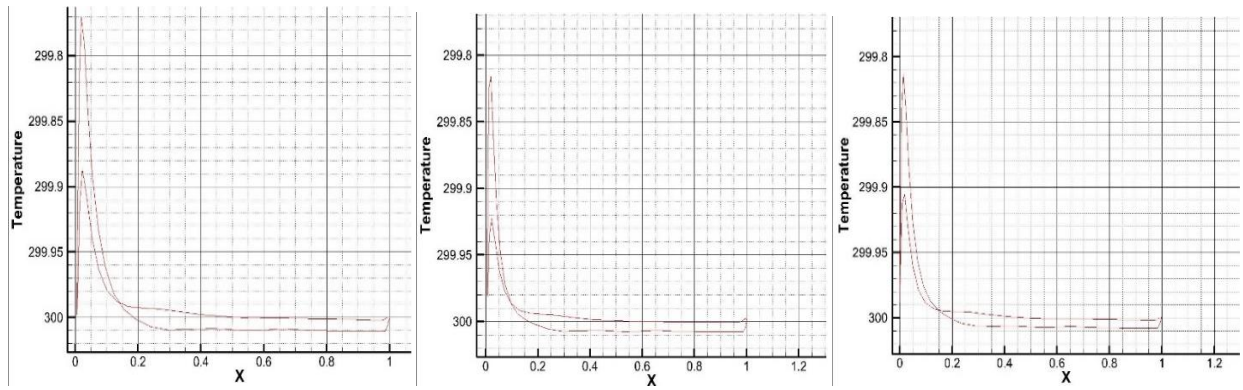
b) 0.25R (GP 13º, GP 12º, GP 11º; from left to right)
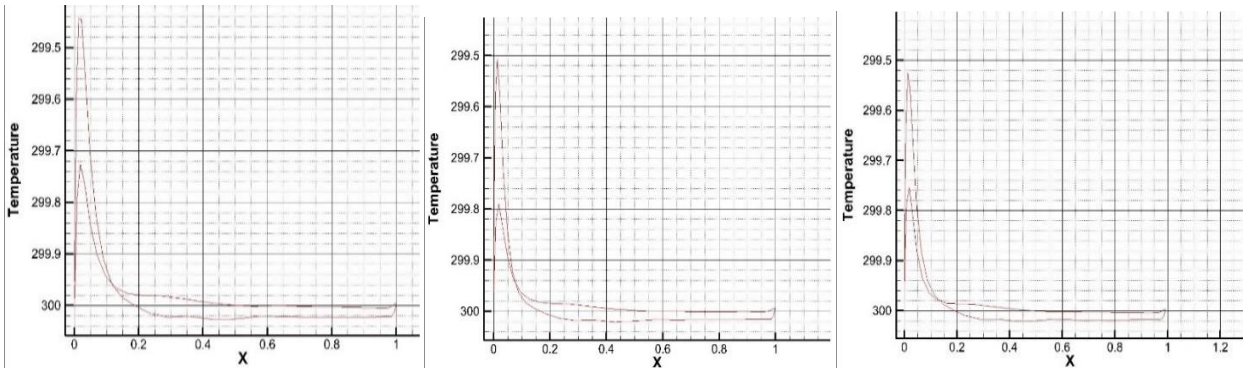
c) 0.50R (GP 13º, GP 12º, GP 11º; from left to right)
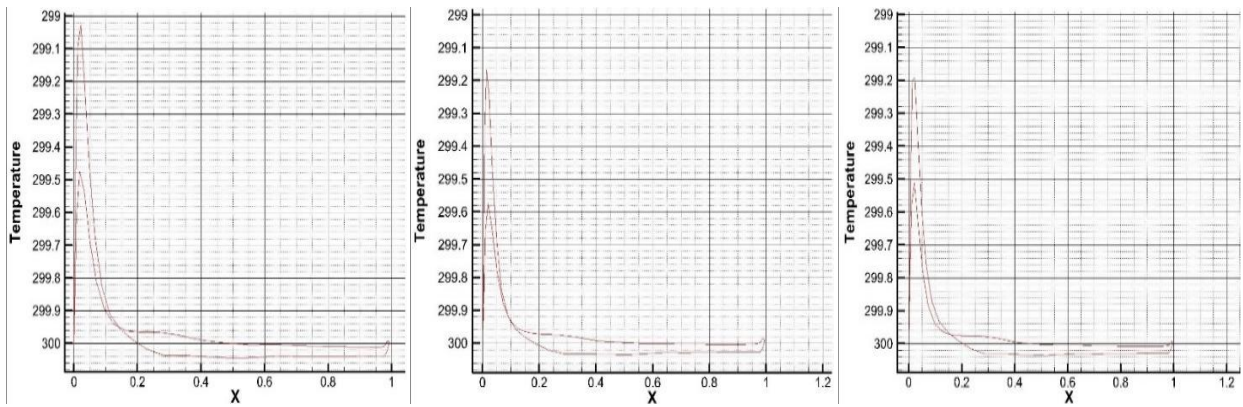
d) 0.75R (GP 13º, GP 12º, GP 11º; from left to right)
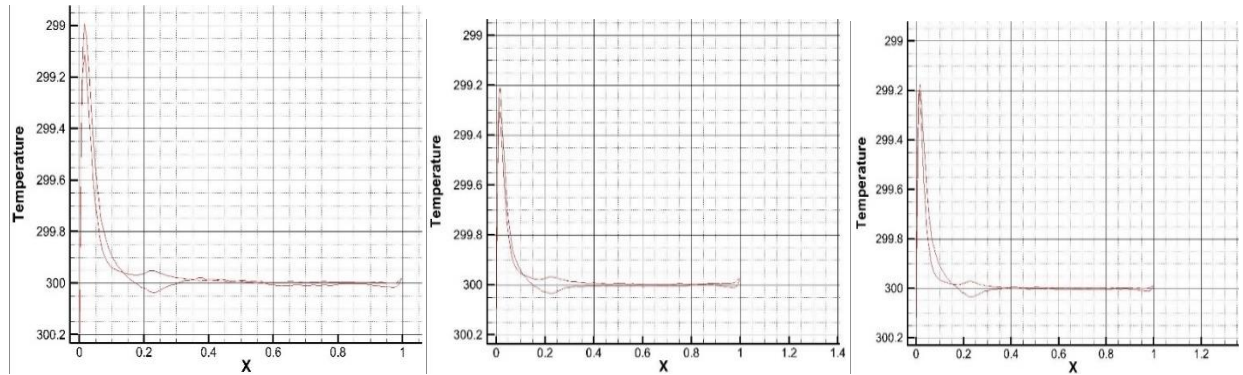
e) 0.99R (GP 13º, GP 12º, GP 11º; from left to right)

Fig. 13 Temperature distribution at a) 0.06R b) 0.25R c) 0.50R d) 0.75R e) 0.99R

B. Comparisons of Blade Thrust and Pressure Distribution at Different Pitch Configurations

a) GP 13°   b) GP 12°c)   GP 11
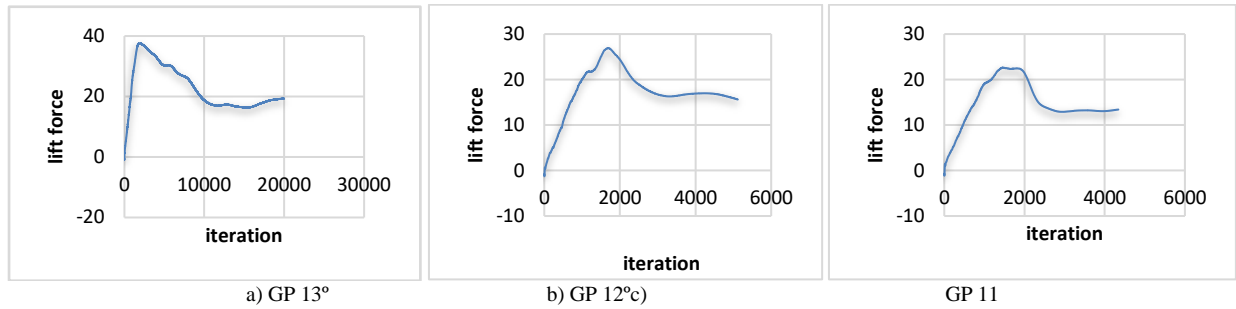
Fig. 14 Lift force of the rotor blade

It can be observed from Fig. 14, that the lift force at pitch GP 12° is easily converged and shows overall better results than the GP 13° and 11° pitch configurations. The pressure distribution on the upper and lower surface of the rotor blade surface is illustrated in Fig. 15 and 16 respectively.

The pressure distribution measured at different radius of the rotor blade with different pitch configurations are depicted in Fig. 17. It is observed that the pressure difference between the lower and upper surface of the rotor blade is higher at GP 12° than the GP 11° and GP 13° pitch configurations.

a) GP 13°   b) GP 12°   c) GP 11°
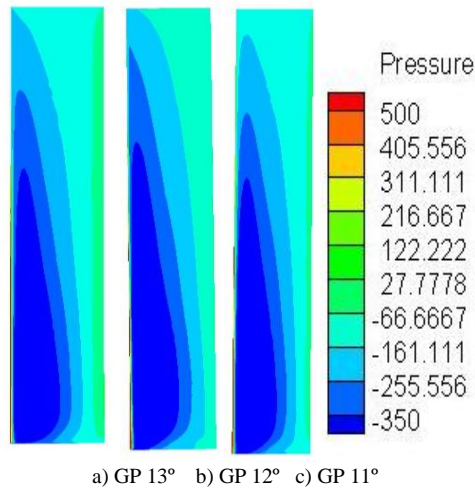
Fig. 15 Pressure distribution on the upper surface of the rotor blade

a) GP 13°   b) GP 12°   c) GP 11°
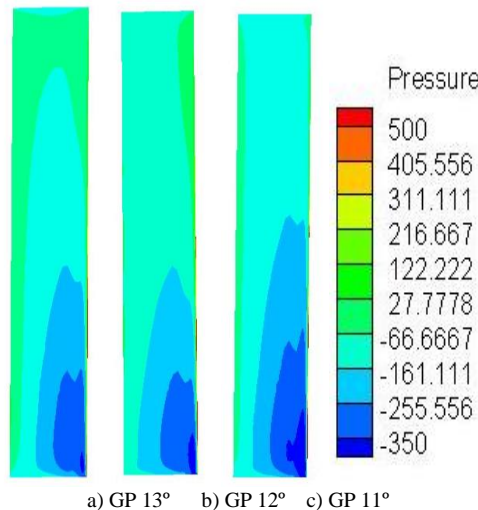
Fig. 16 Pressure distribution on the lower surface of the rotor blade
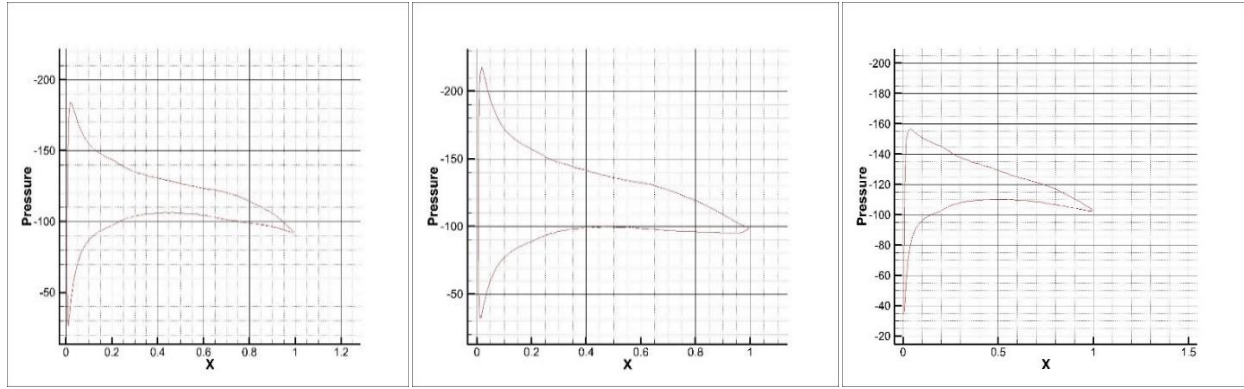
a) 0.06R (GP 13º, GP 12º, GP 11º; from left to right)
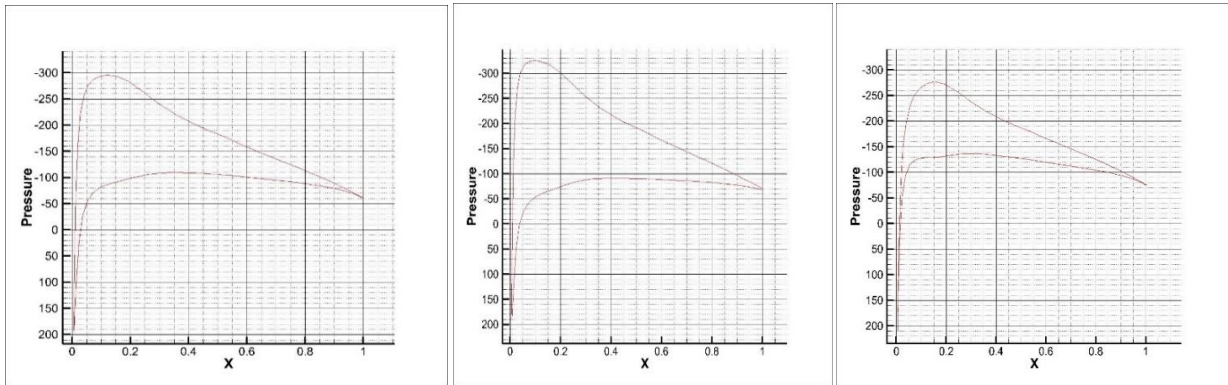
b) 0.25R (GP 13º, GP 12º, GP 11º; from left to right)
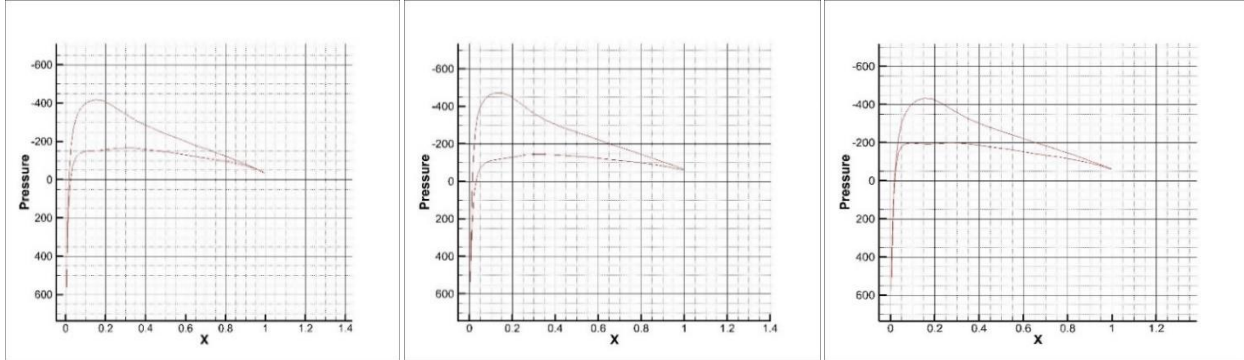
C) 0.50R (GP 13º, GP 12º, GP 11º; from left to right)
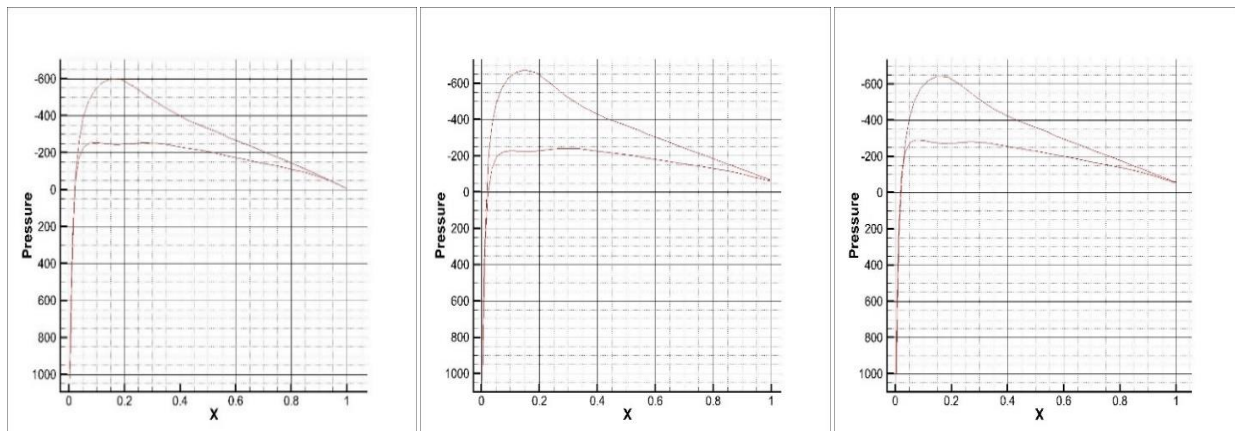
d) 0.75R (GP 13º, GP 12º, GP 11º; from left to right)
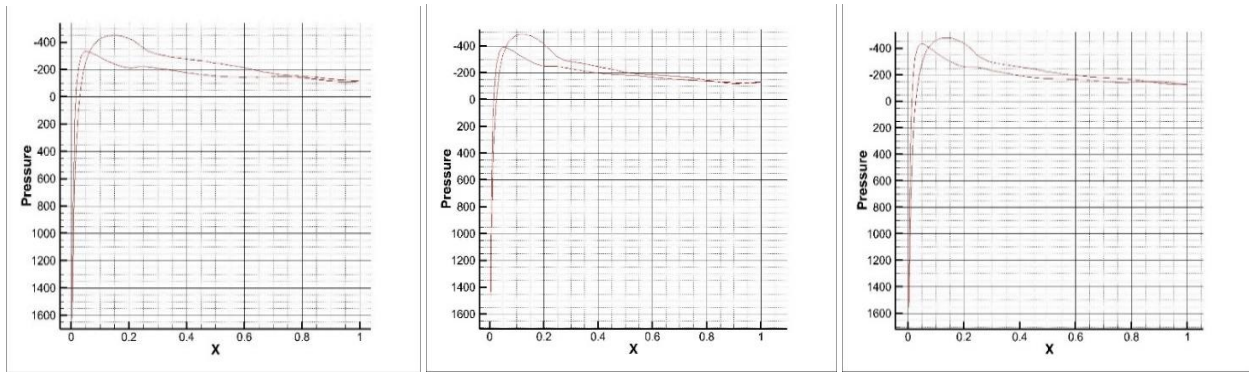
e) 0.99R (GP 13º, GP 12º, GP 11º; from left to right)

Fig. 17 Pressure distribution at a) 0.06R b) 0.25R c) 0.50R d) 0.75R e) 0.99R

C. Comparisons of Velocity Streamline at Different Pitch Configurations

The free stream velocity and pressure distribution around the blade, are depicted in Fig. 18. It can be observed that the free stream behavior near the blade at GP 12º is much more convincing than the other two pitch configurations.
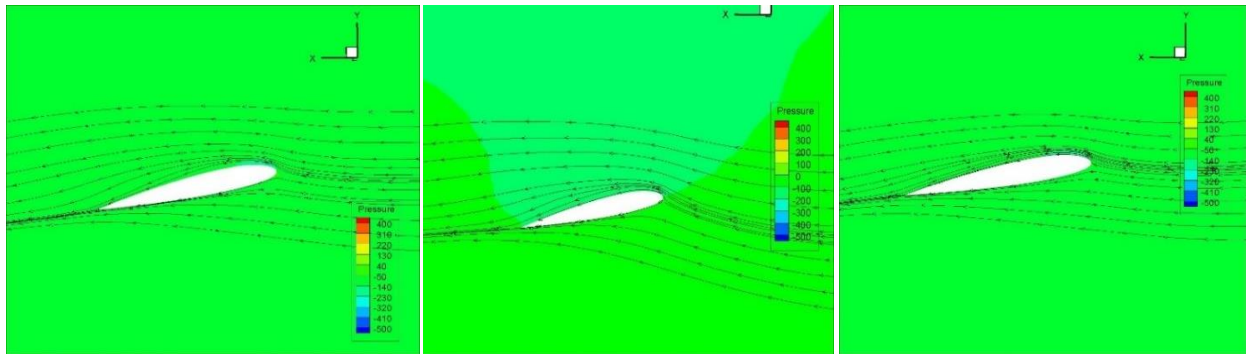
a) 0.06R (GP 13º, GP 12º, GP 11º; from left to right)

b) 0.25R (GP 13º, GP 12º, GP 11º; from left to right)

c) 0.50R (GP 13º, GP 12º, GP 11º; from left to right)

d) 0.75R (GP 13º, GP 12º, GP 11º; from left to right)
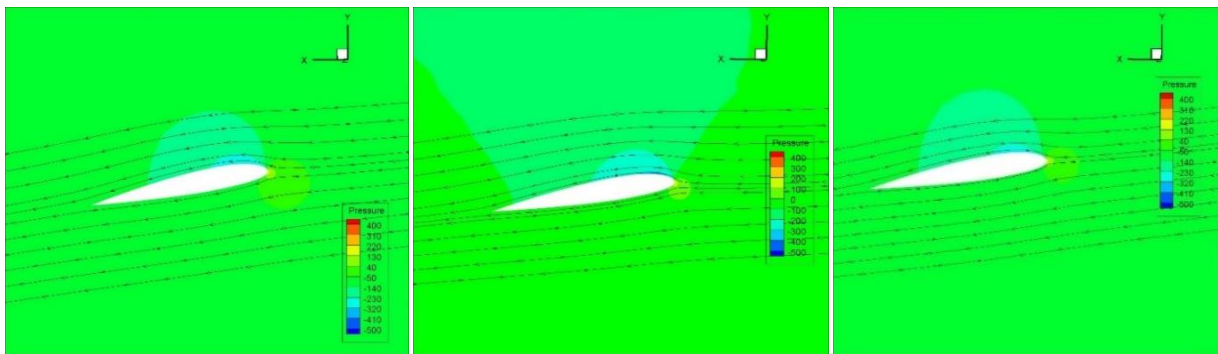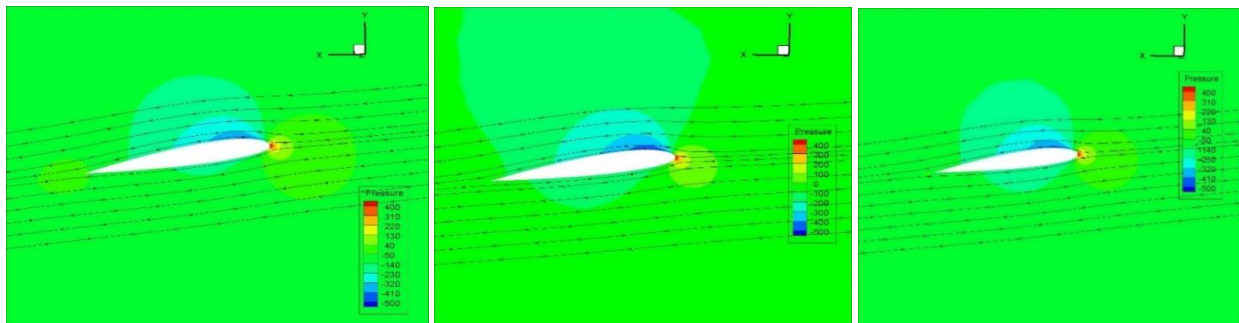
e) 0.99R (GP 13º, GP 12º, GP 11º; from left to right)
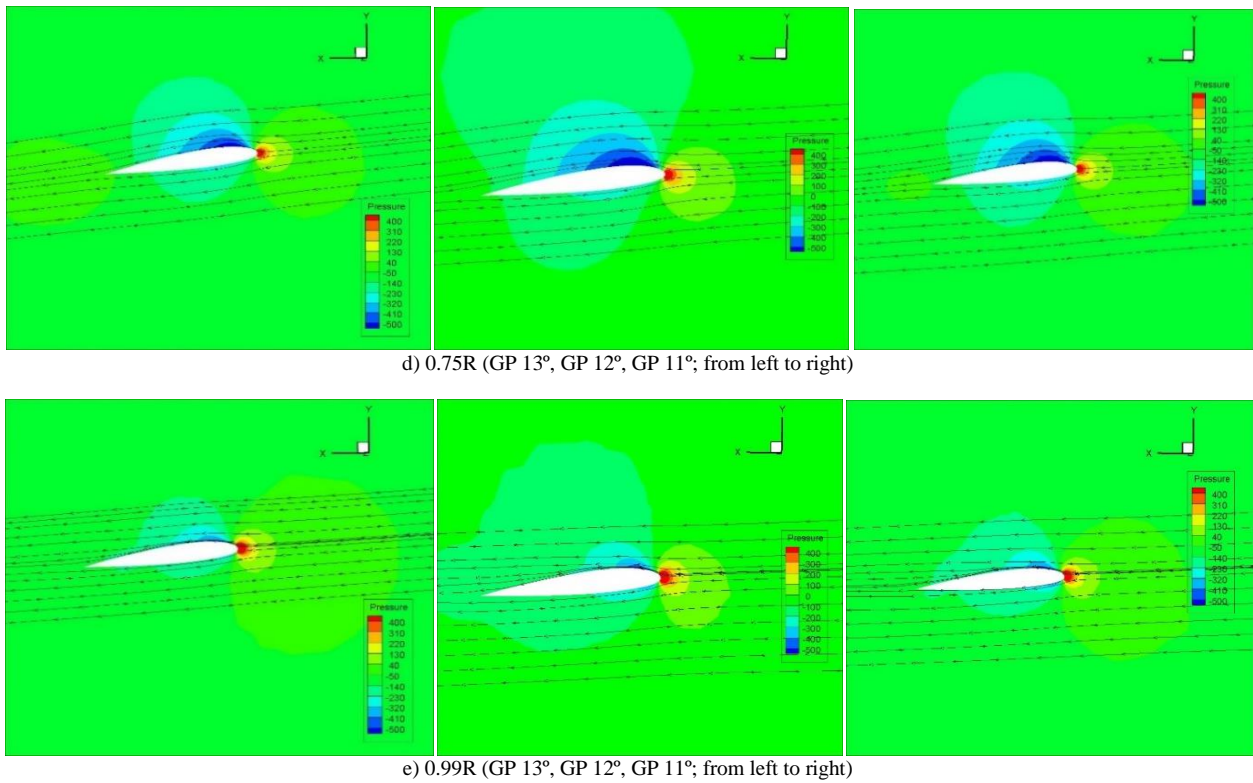
Fig. 18 Free stream velocity streamline and pressure distribution at a) 0.06R b) 0.25R c) 0.50R d) 0.75R e) 0.99R

D. Comparison of X Vorticity at Blade Tip of Different Pitch Configurations

Since the pressure on the lower surface of the rotor blade is more than the upper surface, as a result the fluid around the blade tip flows from the lower surface to the upper surface. This net pressure difference leads to the formulation of the blade tip vortices, as shown in Fig. 19. The x vorticity parameter shows that the vorticity is more at GP12º than GP 13º and GP 11º around the tip of the rotor blade.

a) GP 13º   b) GP 12º   c) GP 11º
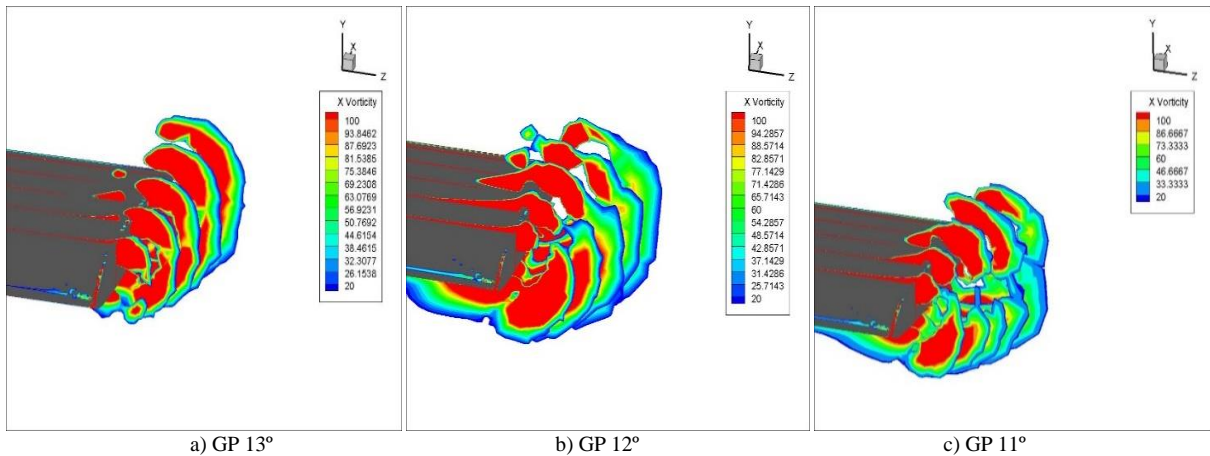
Fig. 19 X Vorticity around the blade tip at different pitches

V. CONCLUSION

Recent uprising demand of MAVs in civil and military usage, has emerged the usage of CFD analysis to evaluate the aerodynamics performance of MAVs at low-Reynolds number. Therefore, a computational investigation is carried out to analyze the rotor blade aerodynamics performance at low Reynolds number at different pitch configurations. The lift force generation, pressure and temperature distribution on the blade surface, x vorticity around the blade tip were obtained from the numerical simulation and used for the comparison between the three different configurations. Finally, it is to conclude that among the three different pitch configurations of the blade, pitch angle at the grip (GP) of 12º shows overall superior aerodynamics performance than the GP 11º and 13º configurations.

REFERENCES

[1]   B. A. Haider, C. H. Sohn, Y. S. Won and Y. M. Koo, "Aerodynamically efficient rotor design for hovering agricultural unmanned helicopter," *Journal of Applied Fluid Mechanics,* Vol. 10, No. 5, pp. 1461-1474, 2017.

[2]   K. T. Lee and C. J. Oh, "Introduction to mission requirement," *Journal of The Korean Society for Aeronautical and,* Vol. 30, No. 8, pp. 156-163, 2002.

[3]   R. Shrestha, M. Benedict, V. Hrishikeshavan and I. Chopra, "Hover Performance of a Small-Scale Helicopter Rotor for Flying on Mars," *Journal of Aircraft,* Vol. 53, July-August, 2016.

[4]   S. P. Yeong and S. S. Dol, "Aerodynamic Optimization of Micro Aerial Vehicle," *Journal of Applied Fluid Mechanics,* Vol. 9, No. 5, 2016.

[5]   M. Drela and M. B. Giles, "Viscous-inviscid analysis of transonic and low Reynolds number airfoils," *AIAA Journals,* Vol. 25, No. 10, pp. 1347-1355, 1987.

[6]   Y. M. Koo, "Performance Comparison of Two AirfoJournal Designs for an Agricultural Unmanned Helicopter," *Journal of Biosystem Engineering,* Vol. 37, 2012.

[7]   G. Shankaran, and M. B. Dogruoz, "Advances in fan modeling: Using multiple reference frame (mrf) approach on blowers," In International Electronic Packaging Technical Conference and Exhibition, Vol. 44625, pp. 259-267, January 2011.

[8]   R. Smith, "Moving Reference Frame for Computational Fluid Dynamics," Symscape, 24, June 2013.